Multi-Scale Study of Spark Plasma Sintered Graphene-SiC Ceramic Composites

Nicholas Wang, Edward Lin, Steven Kotowski, Harmanpreet Singh, Christopher Conner, Alec Roskowinski

Abstract

Silicon carbide ceramics are widely used in various applications for their high strength and favorable thermal properties. The in-situ formation of epitaxial graphene during densification of silicon carbide powder through spark plasma sintering has been recently reported, resulting in claims of novel electronic applications of graphene-SiC ceramic composites. An alternative application for these composites is for mechanically superior ceramics with both high hardness and high toughness properties due to the inclusion of graphene. However, the conditions for graphene formation are inquisitive at best. Additionally, as spark plasma sintering is a relatively new and complex process, sintering behavior of silicon carbide powder due to joule-heating in vacuum and under uniaxial pressing is not clearly understood. This report presents a multi-scale study and model of graphene formation conditions during the spark plasma sintering process of silicon carbide powders. Thermodynamic modeling of silicon carbide constituent vapor pressures with temperature is followed to determine graphene formation conditions. A micro/meso-scale model of grain growth is implemented in Matlab through a Kinetic Monte Carlo and Metropolis algorithm to determine macroscopic sintering parameters. Calculated results deviated from previous research due to a difference in the number of vacancy annihilation attempts, however the general trend was similar in both cases. A macro-scale simulation of spark plasma sintering in COMSOL Multiphysics 4.1 is utilized to model the sintering process and study the mechanisms of electric currents, heat transfer, and densification based on a continuum theory of sintering. The model results are compared to experimental results from silicon carbide samples fabricated through powder mixing and spark plasma sintering at ARL. Due to machine limitations, total densification was not achieved, however graphene was still present in the SiC samples. Mechanical testing, however, was inconclusive and future research in this area would be beneficial in further studying SPS of SiC.

Table of Contents

Motivation

      Spark Plasma Sintering (SPS) is a powder consolidation method in which densification is achieved by the simultaneous influence of electric current and mechanical pressure [1]. The process utilizes pulsed high DC current along with uniaxial pressure to consolidate powders. Powders are placed in a die and heating is affected by passing a current through the die and the sample while a pressure is applied on the powder [2]. A large numbers of papers published during the past decade have demonstrated the importance of the SPS method as a tool for consolidation of powders. The success of the process can be highlighted by a number of noteworthy achievements. Some of which are, smaller grains in sintered ceramic materials [3], a remarkable increase in super-plasticity of ceramics [4], and improved magnetic properties [5].

      Researchers at Penn State have used SPS to develop a method to fabricate a graphene/SiC composite [6]. They are using this method to enhance the electrical properties of Silicon Carbide (SiC), but looking at the exceptional mechanical properties of graphene[7] inspired us to use the same process to exploit the mechanical properties of the graphene/SiC composite. A potential application of such a composite with better mechanical properties can have strong applications in hard body armors, where SiC is mostly used [8].

      The conducted literature surveys [2,9,10] indicate that SPS predictiveness and optimization depend on the availability of reliable process models, which are currently very few and of high demand. This inspired us to design a model that takes into account the macro-scale and micro-scale phenomenon that takes place during SPS. Macro and micro-scale model of SPS for SiC has never been done before. Since SiC is a widely used ceramic, it is important to have a reliable process model to improve the productiveness and optimization of the process. The model could be used for optimization of graphene/SiC composite formation, which has a great potential to be used in body armors. The fact that such a model could be used to tune graphene formation and optimize mechanical properties of products like body armors was the main motivation behind this project.

Materials Science & Engineering Aspects

      The design of this project, which can be subdivided into modeling and fabrication, relies heavily on principles of materials science and engineering. We reached into our previous knowledge of kinetics, thermodynamics, macroprocessing, chemistry, differential equations, and mechanics, among others. We designed a macro and micro scale model of Spark Plasma Sintering (SPS) of SiC. The macro-scale model required the knowledge of flow of electrical current, induced Joule heating, mechanical deformation, densification, and grain growth, while the micro-scale model required the knowledge of coarsening of grains by short-range diffusion across grain boundaries, pore migration and pore coarsening by surface diffusion, vacancy diffusion along grain boundaries, and vacancy annihilation at the grain boundaries. The basics of most of these concepts were covered in kinetics and thermodynamics, while induced joule heating equations were solved based on the knowledge gained from differential equations about heat transfer equations. The micro-scale model produced images of microstructure, which were analyzed using concepts learned in various materials courses.

      The fabrication part of the project was mainly based on the concepts learned in macroprocessing class. The concepts of batching, mixing, and milling were used to have a solution with perfect rheology. The solvent was then evaporated and sample was crushed, batched and sintered. The concepts of sintering and grain growth were also covered in

macroprocessing. The fabricated samples were characterized and tested using materials science based techniques like Raman Spectroscopy and hardness testing.

Previous Work

Modeling of Spark Plasma Sintering (SPS) of SiC has never been done before. The science of sintering has been developing for about 70 years but only few attempts have been undertaken to develop SPS-specific constitutive models of powder consolidation [12-16]; most of the modeling work on SPS has been dedicated to the numerical (predominantly, finite element) analyses of temperature and electric current distributions evolving in the tooling and specimens during SPS processing. Some studies have been done for specimen-free SPS setups [17], which could be useful for thermal expansion calibration of SPS tools but not useful for process optimization. Some studies that do consider powder specimens [18, 19, 20] are based on the assumption of fully dense specimens. All these studies have mostly considered the thermal–electric aspect of the problem and have largely neglected the sintering aspect of the problem. The studies that do consider shrinkage, have associated it with the displacement of electrode punches only and neglected the non-uniformity of the relative density spatial distribution within the specimen's volume [21].

Olevsky et. Al [22] have done study on multi-scale models of sintering using ZnO powder, to successfully predict the dimensional changes during sintering of ZnO bilayers. Olevsky et al. proposed method of a combined meso/macro-scale analysis of sintering kinetics [22] of ZnO and similar powders. In our project, we are following Olevsky's multi-scale approach for SPS of Alumina powders. McWilliams et. al. also follow a similar approach for Tungsten powders where a model was developed by integrating a sintering model into a previously established thermal–electric finite element framework to predict the densification kinetics of the tungsten powder sample.

Design Goals

The project was aimed at developing a multi-scale Spark Plasma Sintering (SPS) modeling of SiC. The aim was pursued by using an integrated approach of combining the continuum theory of sintering with a kinetic Monte-Carlo (KMC) model-based microstructure evolution simulation, and by using our model for the process of in-situ growth of graphene on SiC during SPS. Specific design goal for this project include analytical modeling of silicon sublimation from silicon carbide, analytical proof of COMSOL modeling, macro-scale sintering model in COMSOL, Kinetic Monte Carlo (KMC) code for microstructure simulation, and integration of micro-scale KMC simulation into macro-scale COMSOL model. Beyond the design stage, our team aimed to successfully fabricate the SiC/Graphene composite using SPS to confirm graphene formation and to test the mechanical properties of SiC/Graphene composite.

Technical Approach

Graphene Formation Modeling

The first step in modeling was to address the concern that graphene may be present in currently used, conventionally sintered SiC ceramics such as Hexoloy. The process of epitaxial graphene formation on SiC consists of thermal desorption of Si, which occurs at temperatures and pressures well below that of conventional processing parameters of commercial SiC products. For these processes, SiC powders are sintered at high temperatures (over 1600°C) and pressures (atmospheric to 100MPa).[25] [26] Given these conditions, the inadvertent growth of epitaxial

4

graphene between SiC powders could be feasible and may contribute to the exceptional strength properties of hard ceramics such as SiC.

This process was discussed with Dr. Claire Berger from the Epitaxial Graphene Laboratory at Georgia Tech. From her research and expertise on epitaxial graphene growth on SiC, it was determined that SiC decomposes by selective sublimation of Si at temperatures around 1200°C in high vacuum and/or inert gas atmosphere. As a result of thermal desorption of Si atoms, extra C atoms are left on the surface of SiC, which coalesce to form epitaxial graphene sheets. Ambient conditions will result the reaction of surface carbons to form hydrocarbons or carbon dioxide instead of graphene. Therefore, temperatures of at least 1200°C in high vacuum or inert gas conditions are required for graphene formation.

Micro/Meso-Scale Grain Evolution Modeling

During powder sintering, densification and grain growth occur through temperature and pressure activated mass transport between discrete particles. Thus, a discrete particle model is necessary to accurately simulate grain growth mechanics during sintering. Olevsky et al. proposed a micro/meso-scale of grain growth model based on a Kinetic Monte Carlo (KMC) and Metropolis algorithm that evolves an initial microstructure of discrete grains to simulate sintering densification.[22] We propose a similar micro/meso-scale grain evolution model to determine important constitutive sintering parameters to be utilized in our macro-scale model of SPS.

The KMC and Metropolis algorithm utilized for this simulation was written in Matlab. A 100 by 102 grid is created with each grid space corresponding to a site to be assigned a unique state. States can have values ranging from 0-850. Colored spaces denote unique grain sites while white spaces represent pore sites. This system represents an initial microstructure of 850 hexagonal grains with pores represented by a zero state. The initial microstructure is a uniformly distributed system of 850 grains, as seen in Figure 1. The initial porosity is assumed to be 33%, representative of real green samples used in powder processing. The following processes are simulated by the KMC and Metropolis algorithm: (a) grain growth by short-range diffusion across grain boundaries, (b) pore migration simulating pore diffusion across grain boundaries, and (c) vacancy annihilation as a mechanism of densification during sintering. The following processes were simulated as follows:
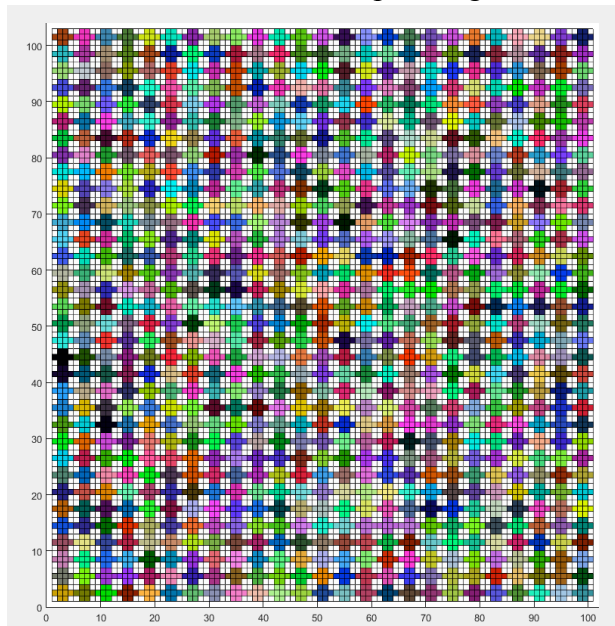

Figure 1. Initial microstructure of 850 hexagonal grains and 33% porosity where colored spaces represent unique grains and white spaces represent pores.

(a) Grain growth is determined by following basic KMC and Metropolis steps. First, the total energy of the system is based on the free and interfacial energies between grain and pore sites and is determined by equation (1):

$$E = \frac{1}{2}\sum_{i=1}^{N}\sum_{j=1}^{8} \begin{cases} \big(1 - \delta(q_i, q_j)\big) \; for \; grain \; sites \\ \big(3 - 3\delta(q_i, q_j)\big) \; for \; pore \; sites \end{cases} \qquad (1)$$

Based on this relationship, the system energy E is total sum of all nearest neighbor energies of each site, N is the total number of sites, q_i is the state of the current site, q_j is the state of the neighbor sites, and δ is the Kronecker delta. The ½ consideration is necessary to avoid double counting of neighbor energies. Based on this equation, the difference in free energy and interfacial energy is taken into account. Neighbor energies are calculated for each site, with like states contributing zero overall energy and dislike states contributing energy depending on the type of interface. The neighbor energy between grains is considered to be 1 while the neighbor energy between pores and grains is considered to be 3. The neighbor energies are then summed over each site to determine the total system energy.

First, the system energy is calculated by equation (1). A grain site, n, is then chosen at random and assigned a new state depending on the states of its neighbors. The KMC algorithm assigns a 1/8 probability of n taking on the state of each respective neighbor. Additionally, the algorithm ensures mass conservation and avoids redundant calculations by allowing n a zero probability of taking on the same state or a zero state. If n is completely surrounded by pores or sites with similar states, a new grain site is considered.

Once n is assigned a new state, the system energy is calculated once more following equation (1). The difference in system energies is then calculated and used to update the microstructure by following the Metropolis algorithm given in equation (2).

$$P = \begin{cases} exp^{\left(\frac{-\Delta E}{k_B T}\right)} \; for \; \Delta E > 0 \\ 1 \; for \; \Delta E < 0 \end{cases} \qquad (2)$$

In the equation, $k_B T$ is an energy scaling factor and determined to be equal to zero in order to accurately simulate grain growth by diffusion[22]. This corresponds to a P value of 0 for an increase in system energy and a P value of 1 for a decrease in system energy. A random number, R, between 0 and 1 is calculated in Matlab. Following equation (2), the new state of n is accepted if R is less than or equal to P and rejected if R is greater than P. With a $k_B T$ value of zero, this correlates to lower energy states being accepted and higher energy states being rejected, which is thermodynamically appropriate.

(b) Pore migration is simulated by choosing a random pore site and a neighboring grain site. The states of the two sites are temporarily exchanged and the change in system energy is calculated using equation (1). The new states are accepted or rejected based on equation (2). Following previous studies, the $k_B T$ value for pore migration is determined to be 0.7, a necessary value to accurately simulate pore migration.[22]

(c) Vacancy annihilation is necessary to simulate densification and requires the presence of a vacancy, which is considered to be an isolated pore site. First, a pore site is selected and its neighbors are analyzed. If it is surrounded by grain sites, it is considered to be a vacancy. The nearest grain boundary site is then determined and the states of the two sites are exchanged. This process simulated vacancy annihilation at grain boundaries.

In order to accurately model grain growth behavior, these processes are carried out at a ratio of 10:10:1 for (a), (b), and (c). The completion of this ratio count as one simulation time step, where a simulation time step is linearly related to real time. Curvature driven grain growth due to the Gibbs-Thomson effect is also taken into account by the nature of the KMC and Metropolis algorithm. Given a curved interfacial grain boundary, grain sites on the concave side of the boundary have a higher interfacial energy than grain sites on the convex side of the grain boundary. Thus, higher energy grain sites will have a higher probability of taking on a new state, eventually causing the grain boundary to flatten. The nature of the algorithm assigns higher energy to higher curvature grain boundaries, which conceptually simulates the Gibbs-Thomson effect.

Based on continuum mechanics and Olevsky's continuum theory of sintering, the microstructural evolution simulated by the KMC and Metropolis algorithm can be utilized to determine macroscopic constitutive sintering parameters.[23] The Laplace pressure, P_L, also called the sintering stress, can be expressed as equation (3):

$$P_L = \frac{\partial F}{\partial P_T} \tag{3}$$

where F is the interfacial-free energy, determined by the pore length, and P is the porosity of the system. Bulk viscosity modulus can also be determined by relating to the Laplace pressure, as shown in equation (4):

$$\psi = \frac{-\overline{P_L}(1-P)}{2\frac{dP}{d\tau}} \tag{4}$$

In this instance, τ is related to the simulation time. Thus, the bulk viscosity modulus and Laplace pressure can be analytically determined based on the continuum theory of sintering.

As the system energy is comprised of the sum of the neighbor energies of each of the 10,200 sites, these calculations require either extensive computing time or power for a large number of timesteps. Thus, parallelization was implemented through Matlab's Parallel Computing Toolbox (PCT). Specifcally, *parfor* loops were used, allowing for parallel computing of independent *for* loops. The simulation was run on a four-core processor desktop computer.

Macro-Scale SPS Model

In order to simulate experimental SPS conditions, a macro-scale model based on the continuum theory of sintering was created in COMSOL Multiphysics 4.1. The continuum theory of sintering by Olevsky is based on continuum mechanics and thermodynamics, and allows for the treatment of a sintered powder compact as a continuous medium. In order to maintain the accuracy of the simulation, sintering parameters determined from the micro/meso-scale discrete particle model are utilized in COMSOL. COMSOL is unique in that it has the ability to couple and simultaneously solve for different physical phenomena using the finite element method. Thus, the functionality of COMSOL is of great convenience for analyzing sintering mechanisms during SPS.

First, a geometry was created in COMSOL to represent the SPS machine at ARL. The SPS geometry is based on values listed in Table 1 and shown in Figure 2. All geometry domains

(e)

were considered to be graphite with the exception of the centermost domain set as α-SiC. Material properties were assigned accordingly and are discussed further in this report.

Table I. SPS dimensions used in COMSOL based on the SPS at ARL.

Sample (a)	
Radius (mm)	12.7
Height (mm)	3.2
Die (b)	
Inner Radius (mm)	12.7
Outer Radius (mm)	15.9
Height (mm)	38.1
Punch (c)	
Radius (mm)	12.7
Height (mm)	50.8
Spacer (d)	
Radius (mm)	47.7
Height (mm)	12.7
Ram (e)	
Radius (mm)	47.7
Height (mm)	25.4

Figure 2. 2-D axially symmetric SPS geometry based on dimensions given in Table I, where (a) is the sample, (b) die, (c) punch, (d) spacer, and (e) ram.
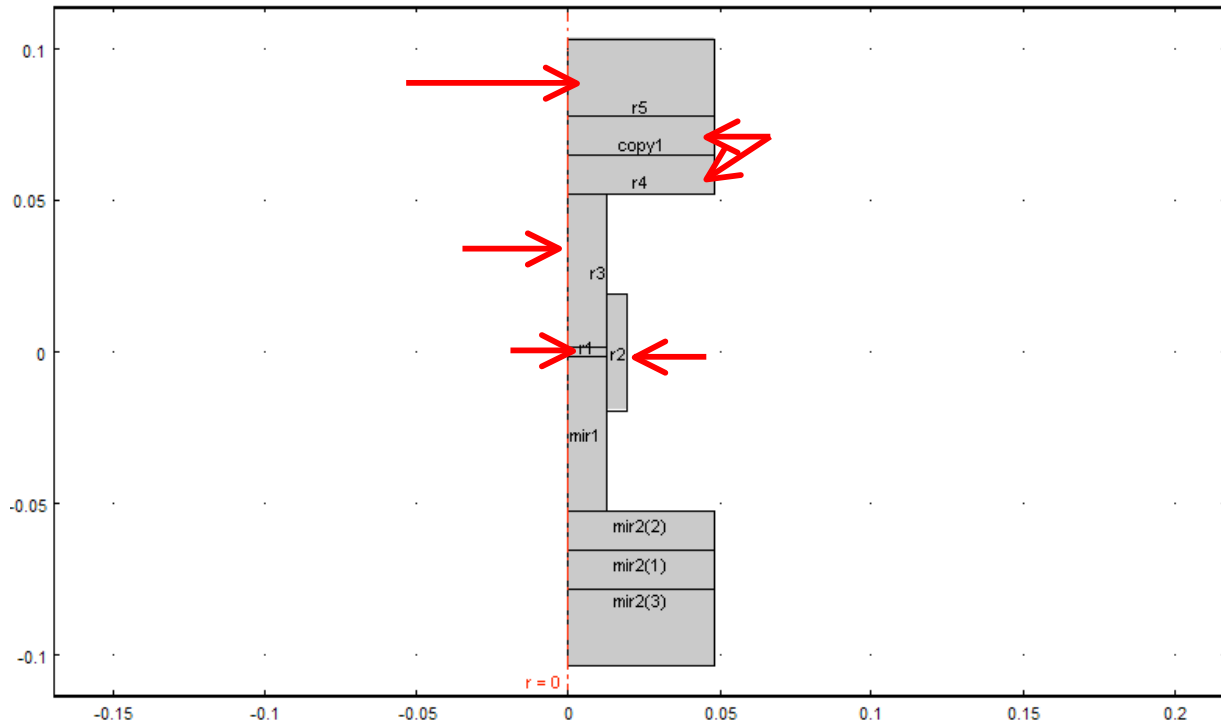
For the SPS simulation, the Joule Heating (electric currents and heat transfer) and Partial Differential Equation (PDE) modules were utilized. The respective modules and assumed boundary conditions will be expanded upon in the following paragraphs.

The Joule Heating module in COMSOL is a combination of electric current and heat transfer analyses. The physics governing electric currents are expressed in equations (5), (6), and (7):

$$\nabla \cdot \vec{J} = 0 \tag{5}$$
$$\vec{J} = \sigma \vec{E} \tag{6}$$
$$\vec{E} = -\nabla V \tag{7}$$

Through these equations, charge conservation in the steady-state is simulated, where $\vec{J}$ is the current density vector, $\vec{E}$ is the electric field vector, V is the electric potential, and σ is the electrical conductivity. Heat transfer by conduction is expressed through energy conservation in time and space, given in equation (8):

$$C_p \frac{dT}{dt} = \nabla \cdot (k\nabla T) + Q \tag{8}$$
$$Q = \vec{J} \cdot \vec{E} \tag{9}$$

In this case, C_p is the heat capacity at constant pressure, k is Boltzmann's constant, T is the temperature in Kelvin, and Q is given as the heat generated due to resistive heating. Combining these two phenomena, the joule-heating relationship in COMSOL is defined as equation (10):

$$\rho C_p \frac{dT}{dt} - \nabla \cdot (k\nabla T) = \sigma |\nabla V|^2 \tag{10}$$

Determination of the assumed initial and boundary conditions in this simulation were important in ensuring accurate results. The initial conditions established for the Joule-Heating module include zero applied electric potential and initial temperature of room temperature, or 293K. The top and bottom of the rams were assumed to maintain a temperature of 293K while an electric potential based on experimental conditions was applied at the top ram. The bottom ram was set as the potential ground. Contact resistance between SPS components was assumed to be negligible. Free surfaces were assumed to be electrically insulating and thermally emissive following the Stefan-Boltzmann law for heat radiation give as:

$$-\boldsymbol{n} \cdot (-k\nabla T) = \epsilon \varepsilon (T_{amb}^4 - T^4) \tag{11}$$

where $\boldsymbol{n}$ is the normal vector to a surface, k is Boltzmann's constant, T is temperature in Kelvin, ϵ is the Stefan-Boltzmann constant, and ε is the emissivity, assumed to be 0.8 for graphite according to the literature values. Heat transfer through convection is disregarded because the sample is sintered under vacuum.

Densification and grain growth are simulated following Olevsky's continuum theory of sintering. Based on this theory, a constitutive sintering equation can be expressed as:

$$\sigma_{ij} = \frac{\sigma(W)}{W} \left[\varphi \dot{\varepsilon}_{ij} + \left(\psi - \frac{1}{3}\varphi \right) \dot{e} \delta_{ij} \right] + P_L \delta_{ij} \tag{12}$$

9

where σ is the uniaxially applied pressure, φ is the shear viscosity modulus, ψ is the bulk viscosity modulus, $\dot{\varepsilon}_{ij}$ is the strain rate, $\dot{e}$ is the shrinkage rate, P_L is the Laplace or sintering pressure, and δ is the Kronecker Delta. $\sigma(W)$ and W are the effective tress for power-law creep and equivalent strain, given by:

$$\sigma(W) = \bar{A}T^m \exp\left(\frac{m\Delta H}{RT}\right)\left(\frac{G}{G_0}\right)^2 W^m \tag{13}$$

$$W = \frac{1}{\sqrt{1-P}}\sqrt{\varphi\dot{\gamma}^2 + \psi\dot{e}^2} \tag{14}$$

In this instance, P is the sample porosity, $\dot{\gamma}$ is the shape change rate, G and G_0 are the grain size and initial grain size, and m, $\bar{A}$, and ΔH correspond to the inverse of the power-law creep stress exponent, a power-law creep coefficient, and the activation energy for power-law creep, respectively. In the context of SPS where the sample is pressed in a rigid die, the expressions for the shape change rate and shrinkage rate, given in equations (15) and (16), simplify to equations (17) and (18) respectively.

$$\dot{\gamma} = \sqrt{(\varepsilon_{rz}^2 + \varepsilon_{r\phi}^2 + \varepsilon_{z\phi}^2) + \frac{2}{3}(\varepsilon_r^2 + \varepsilon_z^2 + \varepsilon_\phi^2) - \frac{2}{3}(\dot{\varepsilon}_r\dot{\varepsilon}_z + \dot{\varepsilon}_r\dot{\varepsilon}_\phi + \dot{\varepsilon}_z\dot{\varepsilon}_\phi)} \tag{15}$$

$$\dot{e} = \dot{\varepsilon}_z + \dot{\varepsilon}_r + \dot{\varepsilon}_\phi \tag{16}$$

$$\dot{\gamma} = \sqrt{\frac{2}{3}}\dot{\varepsilon}_z \tag{17}$$

$$\dot{e} = \dot{\varepsilon}_z \tag{18}$$

This is determined because strain due to power-law creep occurs only in the z direction due to pressing in a rigid die. Given the continuity equation (19):

$$\frac{\dot{P}}{1-P} = \dot{e} \tag{19}$$

the relationship for densification rate, $\dot{P}$ can be derived. The grain growth rate is also simulated and expressed as:

$$\frac{dG}{dt} = \frac{k_0}{3G^2}\left(\frac{P_c}{P_c+P}\right)^{\frac{3}{2}}\exp\left(\frac{-Q}{RT}\right) \tag{20}$$

where k_0, P_c, and Q are grain growth parameters referenced in literature. This grain growth equation is formulated by Olevsky and takes into account the effect of grain boundary pinning.[21] These equations are implemented in COMSOL's PDE module, which is able to solve partial differential equations by the Runge-Kutta method of the fourth order. In this instance, P_c is taken to be equal to 0.05 following Olevsky et al.'s methods. The initial grain size and porosity is assumed to be equal to 1 μm and 33%, to reflect experimental conditions and the micro/meso-scale simulation, respectively. These equations, boundary conditions, and parameters are factored into COMSOL finite element analysis to calculate the temperature profile and densification during SPS.

Material parameters for graphite and SiC in COMSOL were determined from the literature. Specifically, the material properties of POCO ZXF-graphite were referenced from the vendor literature[27 28]. Temperature dependent properties of SiC powders were taken from several souces[12-14,21-23]. While the literature values are fairly accurate and agreed upon, they fail to take into account the effects of densification, which may be cause for error in future simulations.

a)

b)
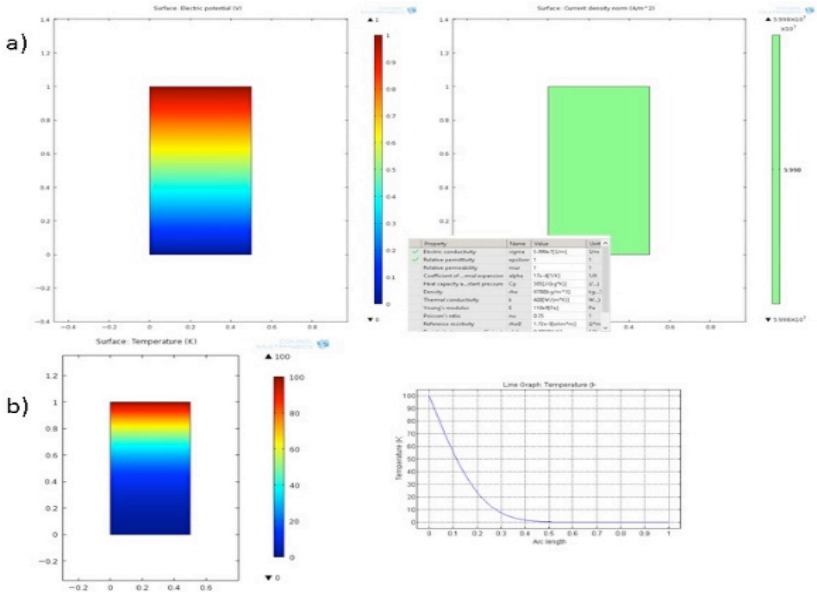
In order to authenticate the results from Comsol, simple verification tests were conducted. These tests include a 2-D analysis of the electric currents and heat transfer modules. The test geometry was a simple, 2-D 1 meter by 1 meter square made of copper. The electric currents test assumed initial conditions of zero electric potential and 1V applied at the top of the square. According to the calculations, the resulting current density should be uniform and equal to the electrical conductivity of copper, as seen in Figure 3a. Solving the energy conservation equation for heat transfer, the resulting temperature profile should reflect a function that is similar to a cosine wave, with high temperatures towards the heat source and a decreasing temperature profile along the material, which can be seen in Figure 3b. The verification tests for joule-heating were successful as Comsol accurately predicted current density and thermal gradients. As a verification of the densification equation solved for in COMSOL, as well as a final verification test for joule-heating, the SPS model by Olevsky et al. is recreated in COMSOL and the temperature and densification profiles are compared to their simulation.[21] From the results of this verification, our model replicates their findings, indicating that our model is working correctly.

Fabrication

The design aspect of our project focused on the modeling of the sintering process. Thus the prototype was used to confirm the accuracy of the model and was fabricated based on the specifications of Terrones' patent.[36] The raw chemicals required included 2 μm α-phase Silicon Carbide powder (99.8%), <1 μm α-phase Aluminum Oxide (99.9%), and <10 μm α-phase Yttrium(III) Oxide (99.99%). First the powder was measured using a digital balance, we used 24.4g of SiC with 2 wt% of Al2O3 (.525g) and 5 wt% of Y2O3 (1.312g) for each batch. We placed these batches in individual bottles along with 150 mL of ethanol. To each bottle we added 100 grams of milling material, in this case yttria stabilized zirconia milling balls. The bottles were placed on an attrition mill for 27 hours before the slurry was removed. This was then placed in an oven at 100°C and left overnight. The powder was then crushed using a mortar and pestle.

We had ample powder so more batches were not necessary. The powder was taken to the Army Research Lab at the Aberdeen Proving Grounds. There we used a Spark Plasma Sintering machine to consolidate our powder. A total of 4g of powder was put into a 1 inch diameter graphite die. The die was placed in the machine and the temperature profile laid out in the patent was implemented. This called for a heating rate of 133°C/min up to 1400°C, 100°C/min from 1400°C to 1500°C, 90°C/min from 1500°C to 1680°C, 45°C/min from 1680°C to 1770°C, 30°C/min from 1770 to 1800°C, and finally the temperature was held at 1800°C for 5 minutes. All of this was to occur in a 4 Pa vacuum, with a uniaxial pressure of 50 MPa, using a pulsed direct current. This was not exactly the case however, as with be discussed later on in results and discussion.

Characterization and Testing

After the successful fabrication of our SiC samples, our primary goal is to confirm the formation of graphene in each of our samples. Raman spectroscopy is an excellent tool that is commonly used to identify compounds in a material. This form of spectroscopy operates under the principle of inelastic scattering of monochromatic light. The material is placed under a laser, where the light interacts with rotational vibrations, phonons, and other excitations that shift the energy of the light. These energy shifts are then correlated with bond energies, thus determining the material composition. We scanned multiple points over the surface of each sample, including duo scans which scanned over an area of 40 x 40 microns and averaging the sample composition.

With confirmation of successful graphene formation, we can then begin probing the mechanical properties of our samples. SiC is known for its exceptional hardness, therefore the hardness of our samples was measured as to investigate the potential mechanical advantages of our sample. The samples were first polished with SiC polishing paper to prep for hardness testing. A Vickers Hardness Test was performed on our samples, both due to its uniformity and the expected hardness of our samples is too high for other indenters. No less than three indents were made per sample with 30kgF and a ten second hold. The Vickers hardness number is then calculated by the formula:

$$HV = \frac{F}{A} \approx \frac{1.8544F}{d^2}$$
(21)

where F is the force in kgF and d is the average diagonal of the indent. The resulting HV can then be compared to known values for SiC to determine the mechanical potential of spark plasma sintered SiC.

Ethics and Environmental Impact

Silicon carbide graphene composites have potential use in various structural and electrical applications. Our group focused more on the improvement of mechanical properties for the purposes of something like body armor but such a composite may find use in semiconductors, photovoltaics or the automotive industry. The main goal of our project was to design a model capable of demonstrating the creation of graphene in Silicon Carbide via Spark Plasma Sintering. The model in and of itself has no real ethical or environmental impact. In terms of prototyping such a material also has little environmental and ethical impact. According to the MSDS statements SiC, Al2O3, Y2O3, and ethanol all have very little environmental impact. As with most chemicals they simply should not be allowed to penetrate top soil or be allowed to enter

sewage or waterways. The energy required to run the SPS machine is not significant either especially when compared with the energy consumption of standard sintering methods. In terms of ethical impact the material would benefit electrical and structural applications and there would be very little negative societal impact from the technology itself. So long as the powders are handled with care they present no health concerns. Overall this project has very little ethical or environmental impacts. There may be increased danger as the process grows to a larger scale, however the technology to produce at high volumes is not readily available. The disposal of these materials depends on local regulations but should not require special treatment. Lifetime may vary greatly depending on the application although with improved electrical and mechanical properties it should last longer than many of the materials it would replace. Worn out device can be disposed of similar to the raw materials themselves. As an organic compound Silicon Carbide would be disposed of like other naturally occurring ceramics and would only be difficult due to the high hardness of the compound.

Intellectual Merit

Macro and micro-scale model of Spark Plasma Sintering (SPS) for SiC has never been done before. Since SiC is a widely used ceramic, it is important to have a reliable process model to improve the productiveness and optimization of the process. Modeling of SPS process in general is also in its initial stages where only a few attempts have been made to develop SPS-specific constitutive models of powder consolidation [12-16]; most of the modeling work on SPS has been dedicated to the numerical (mostly finite element) analyses of temperature and electric current distributions evolving in the tooling and specimens during SPS processing. Most of the SPS studies till date are focused on SPS tools and are not useful in process optimization.

In our design, we not only designed the macro-scale model of SPS that couples electrical, thermal, stress-strain, and densification, using COMSOL, but also designed a micro-scale model using Kinetic Monte Carlo algorithm to evolve our initial microstructure to simulate grain growth and evolution during sintering. Our goal is to use our model for the process of in-situ growth of graphene on SiC during SPS. Growth of graphene on SiC for improving the mechanical properties of SiC has never been done before. Graphene has been grown on SiC before to enhance the electrical properties of SiC [6]. We have used our process parameters to fabricate a SiC/Graphene composite and results from Raman Spectroscopiy confirmed the formation of Graphene on SiC.

Broader Impact

Ceramics are inherently hard to work with. They are brittle, hard, and extremely flaw sensitive. What is more, are the effects of processing methods on ceramic properties. Much of the kinetics and thermodynamics of many sintering processes are still unknown, and thus cause endless time, material, and financial waste. Electric current assisted sintering such as SPS has become a growing method of quickly forming difficult to sinter ceramics, such as SiC, yet especially little is known about this process.

Our study to model SPS of SiC can help to fill in the gaps of knowledge in this process. Greater, more repeatable production of SiC and SiC-graphene composites will come from a greater base of knowledge started by this project. These materials will undoubtedly continue to grow in the electronic and body armor fields, pushing forward technology and saving countless lives.

Results and Discussion

Graphene Formation Modeling

        In order to confirm Dr. Berger's conclusion, analytical modeling of Si sublimation from SiC was conducted, following the process outlined in recent research from a group at the Naval Research Lab.[29] Gaskill et al. portray Si sublimation by analyzing the vapor pressures of each SiC component at varying degrees of temperature and pressure. Specifically, they compile data from thermodynamic analyses of the gas phases at the dissociative evaporation of SiC conducted by Lilov.[34]

        Experimental data from an updated study published by Lilov two years later was compiled and analyzed for this model.[30] Lilov's study compiles research from other groups to determine the gas phases over different polytypes of SiC, specifically alpha and beta. Since alpha SiC powder will be used for fabrication, the data for alpha SiC was analyzed and plotted in Figure 4. Our results correspond closely to those from Gaskill et al. and support Dr. Berger's research. From the model, it can be determined that epitaxial graphene formation on SiC is possible between 1200°C-2200°C depending on the vacuum pressure. This dispels the original concern that graphene could inadvertently form during conventional processing of Hexoloy and supports our goal of fabricating a graphene-SiC ceramic composite.
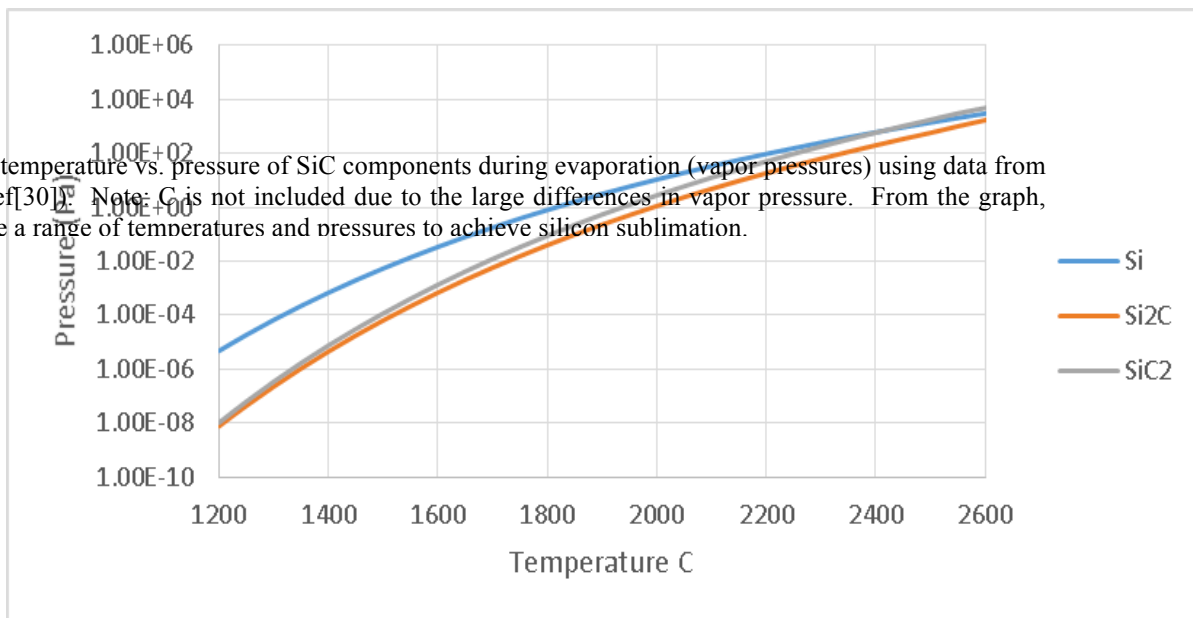

Figure 4. Plot of temperature vs. pressure of SiC components during evaporation (vapor pressures) using data from Lilkov (From Ref[30]). Note: C is not included due to the large differences in vapor pressure. From the graph, one can determine a range of temperatures and pressures to achieve silicon sublimation.

Micro/Meso-Scale Grain Evolution Modeling

        The Matlab simulation was run for 40,000 Monte Carlo timesteps, where an image of the microstructure would be output at every 2,500 timesteps. In Figure 5, the progression of the simulation is shown from the initial microstructure, at 20,000 timesteps, and at 40,000 timesteps.
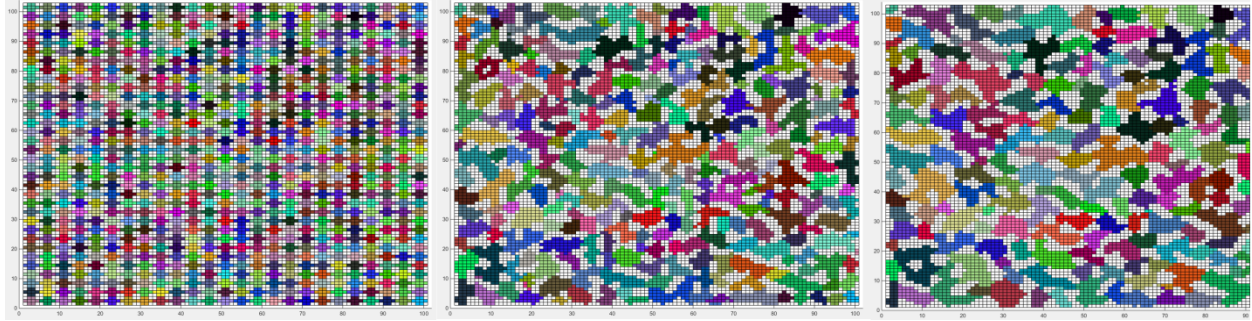
Using ImageJ, the relative porosity could be calculated by subtracting the area of the pores, or white sites, from the total area, or white sites and colored sites. This would show the densification of the grains over time. Figure 6 depicts the densification from 0 Monte Carlo timesteps to 40,000 timesteps, as well as the simulation data from Olevsky et al.

The densification follows the same trend as the data from Olevsky et al.; however, this occurs at a much slower rate. The densification obtained from the Matlab model did not reach 80% relative density at 40,000 timesteps while Olevsky et al. were able to achieve nearly 95% relative density. This may be due to the Matlab simulation only accounting for a grain growth to pore migration to pore annihilation attempt ratio of 10:10:1. Olevsky et al. noted that this ratio changed to 10:10:n, where n is chosen to "ensure the simulation of vacancy annihilation in proportion to diffusion along the length of the grain boundary." As such, pore annihilation in the Matlab simulation occurred much less frequently per Monte Carlo timestep, and may account for a slower rate of densification.

Figure 6. Densification as a function of monte carlo timesteps (matlab simulation data compared to Olevsky data from ref [22].
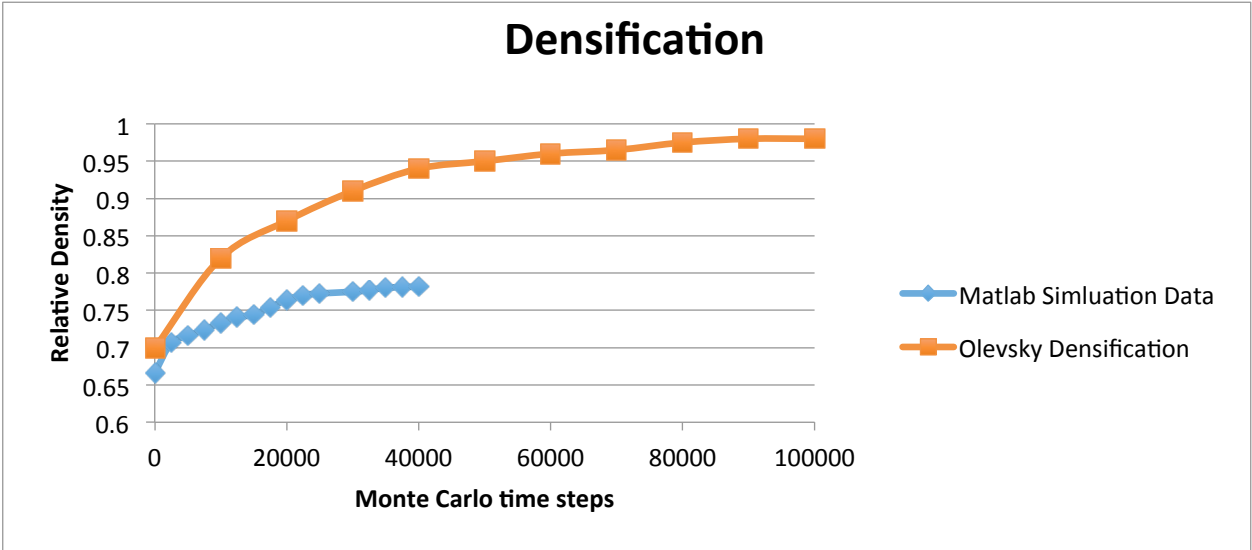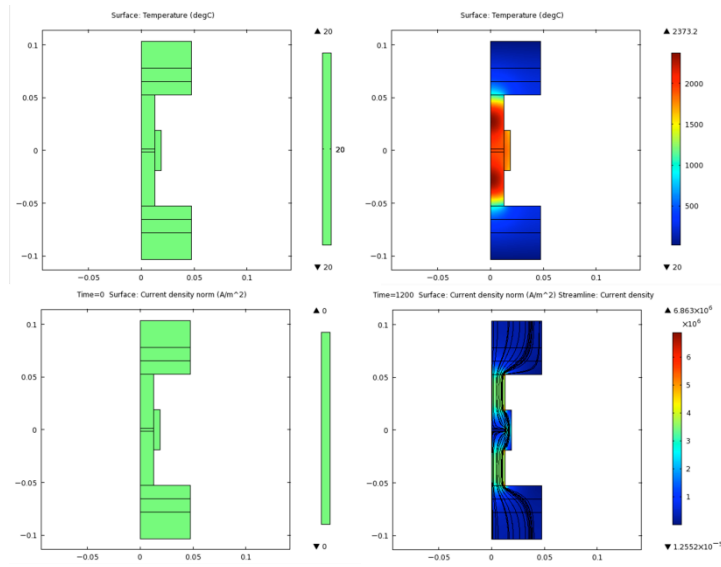
Macro-Scale SPS Modeling

SPS simulations in COMSOL were compared to experimental results from SPS runs at ARL. From powder and sample measurements, the initial grain size and porosity were determined to be 0.2 μm and 56% respectively. Additionally, the sintering equations (12)-(19) were combined and simplified, resulting in a differential equation for densification given in equation (20):

$$\dot{P} = (1-P)\left[\left(\frac{\overline{\sigma}-P_L}{AT^m\exp\left(\frac{m\Delta H}{RT}\right)}\right)\frac{\sqrt[m-1]{1-P}}{\sqrt[m+1]{\frac{2}{3}\varphi+\psi}}\right]^{1/m} \tag{21}$$

This relationship is solved for in COMSOL using the Runge-Kutta method to the fourth order. The power-law creep parameters for SiC required for the densification equation were determined from a combination of literature reference and calibration. ΔH and m are the activation energy for power-law creep and the inverse of the stress exponent fact, which can be found in several references.[31 32] The parameters ΔH and m were calibrated within the range of given literature values in order to more accurately fit the simulation results to the experimental results. The material parameter, A, is not as well studied and required calibration on our part in COMSOL to accurately represent the densification kinetics of the experiment. The combination of power-law creep parameters for SiC that most accurately simulated experimental measurements were values of 0.28, 896 kJ/mol, and 0.25 $Pa \cdot s^m/K^m$.

The SPS simulation was used to calculate the temperature, current distribution, and densification kinetics for simulation times of 1800 seconds and 7770 seconds. Temperature and current distributions can be seen in Figure 7(a) and (b). From the simulations it is apparent that the graphite punches increase in temperature due to joule-heating, which in turn increases heat flow to the sample. Additionally, due to the high electrical resistivity of SiC, electric current flows around the sample and through the graphite die. Thus, resistive heating of SiC is not a contributing factor to heat generation during SPS. This conclusion supports several similar studies regarding SPS of ceramic powders with high electrical resistivities.[33 34]

The SPS simulation results were also compared to the experimental conditions used for sintering at ARL in order to determine the accuracy of our model. Shown in Figure 8 are the voltage, temperature, and density profiles of the simulation results and the experimental results for both runs. The voltage profile is

Figure 7. (a) Temperature distribution of the SPS machine at 0s and 1200s and (b) Current distribution and path of the SPS machine at 0s and 1200s.

1)

uploaded into COMSOL and used to determine the temperature profile through calculations by COMSOL's multiphysics modules. These results match closely with the experimental results, with the exception of the densification. Additionally, the temperature profile deviates a small
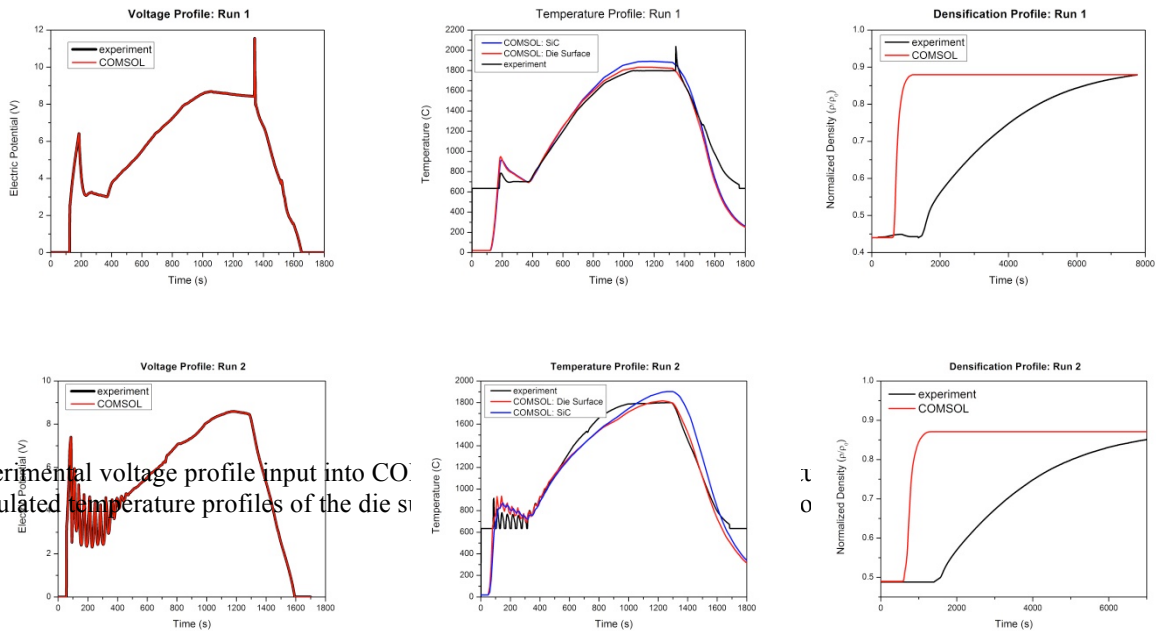
2)

Figure 8. (left) Experimental voltage profile input into CO[...]
[c]ompared to the simulated temperature profiles of the die su[...]

amount between the experimental values and the simulated values.

These deviations can be attributed to several factors. In the experimental sample, Al_2O_3 and Y_2O_3 were included as sintering additives in minute amounts. These compounds were not considered in the simulation and may have contributed to the densification deviations. Additionally, due to the inclusion of these additives, taking into account composite powder material considerations for heat capacity, thermal conductivity, and electrical resistivity would result in more accurate calculations. While graphene should form towards the end of process, its influences may also affect the heat and electric current measurements. Another aspect that is not considered is the effect of porosity on the properties of SiC. Inclusion of porosity influences would also contribute to more accurate simulations. Also state in the technical approach is that the phenomenon of contact resistance between SPS components is not considered, which would most likely affect the resistive heating results. Finally, it is noted in other studies that several power-law creep parameters are temperature dependent, although they are considered to be constant for our purposes.[35]

Additionally, the experimental sintering process at ARL resulted in deviations that were not accounted for in the simulation. Surface temperature readings are measured by a pyrometer in order to determine the sample temperature. However, as shown in the previous figures, thermal gradients exist along the SPS tooling, resulting in the sample being at a higher temperature than anticipated. Initial concern was shown regarding the displacement readings from the SPS due to thermal and electrical noise. The SPS machine at ARL was also incapable of applying the sufficient pressure of 50MPa to fully densify the sample. It instead applied a constant pressure of approximately 1MPa. As the densification formula in equation (21) models

17

pressing in a rigid die, the small applied pressure value may have caused deviations in the densification results. Another observation that seems physically inexplicable is that, according to the experimental measurements, densification occurs after the highest temperature has been reached instead of during. Thus, future work into modeling of SPS densification of SiC powders using COMSOL is necessary.

Fabrication

The result of our fabrication was 3 discs each with 1 inch diameter and 1/8 inch thickness. These samples were confirmed to contain graphene via Raman spectroscopy, these results will be shown in the characterization section. The fabrication was delayed due to a processing issue of one of our order forms, this was caused by the power outage. It was also delayed because the SPS machine broke down and took several weeks to be repaired. In addition some of the steps laid out in the patent were changed as a result of resource and time constraints. For instance the patent used .78 μm SiC powder while we used 2 μm. However, we milled our samples for 27 hours while the patent only called for 2 hours in order to ensure a smaller size. The milling process called for 70g of silicon nitride milling balls but these were not available so we instead used 100g of yttria stabilized zirconia. The equipment to sieve our samples was not available but with the additional milling time this was considered unimportant. This assumption was correct as our final particle size was around .2 μm, much lower than the size of the sieve and the powder used in the patent. During the SPS process we ran into several issues that required us to diverge from the process in the patent. For instance the first heating rate ended up blowing out the thermocouple. Due to this we had to use the pyrometer to measure the temperature while sintering. This required us to add an additional step, namely an initial soak at 700°C. This is because the SPS utilized a high temperature pyrometer which cannot measure temperatures below 650°C. By first soaking the sample we ensured a better control of our thermal process. Another change that occurred was that we could not apply a 50 MPa uniaxial pressure. This is because at 1800°C the dies were likely to break. Any increase in pressure would almost certainly have broken the die so we did not attempt any runs at this pressure. We were initially hoping for more samples and had more than enough raw materials. However, the sintering process took much longer than we were lead to believe, about 1 sample per day. We had also hoped to create a purely SiC sample using hot isostatic pressing. Unfortunately the SPS could not manage the pressure and temperature to do this and a hot isostatic press was not available. Due to time and equipment restraints we ended up with 3 samples. These samples were successful however, as they confirmed that the process created graphene and we were able to use them to confirm out model.

Characterization and Testing

With one of the main goals of this processing being the formation of in-situ graphene, the results from the Raman spectroscopy were extremely successful. As shown in the figure, there are clear peaks around 1500 cm^{-1} and 2700 cm^{-1} that are indicative of graphene. Particularly, a pronounced peak around 2700 cm^{-1} is characteristic of single layer graphene. SiC peaks are also shown at 796.5 cm^{-1} and 973 cm^{-1}.
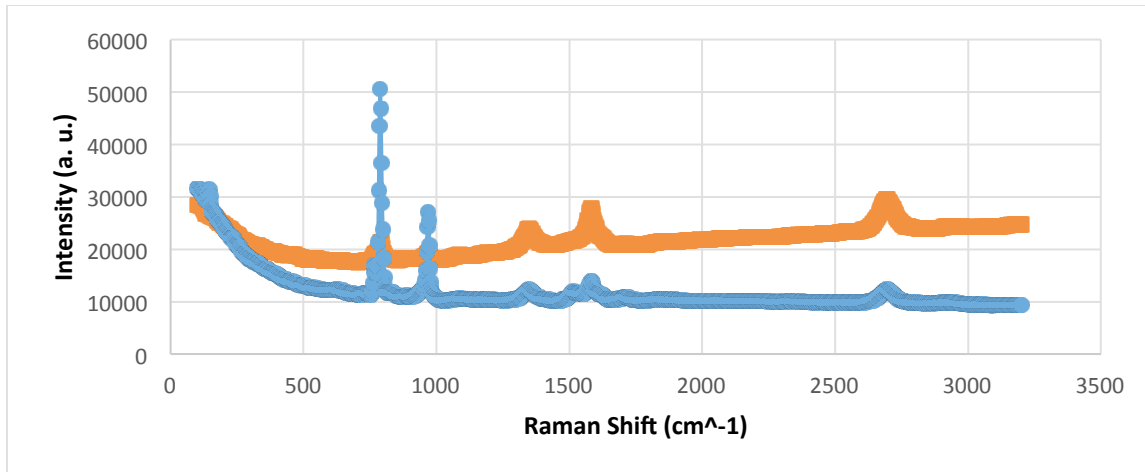
Figure 9: Intensity vs. Raman Shift plot of sample 4 (blue) and sample 7 (red).

The Raman results clearly support the in-situ formation of graphene through our electric current assisted sintering method. This is hopeful for the future production of graphene-SiC composites in a single step process. Additional research remains to be done to further investigate the microstructure of this composite, and its effect on its properties. Raman mapping may be performed in the future to more clearly see the spread of graphene throughout the samples. This can be coupled with SEM imaging to gain a complete picture of the morphology of this composite, including graphene platelets and grain size, distribution, and density.

The Vickers hardness testing revealed interesting results. SiC ceramics often have a Vickers hardness of at least 2000HV, but our samples resulting in much lower values given in the table.

Table 2: Vickers hardness test results for Samples 4 and 7

Hardness (HV)	
Sample 4	Sample 7
1760	820.7
1436	598.8
1347	820.7

The reason for these low hardness results is likely due to the processing conditions. We were unable to sinter our samples under the desired 50Mpa of pressure due to machine limitations at ARL. Instead we had to use nearly pressure-less sintering under less than 1MPa, resulting in less dense samples. According to Terrones' patent, applied pressure is required to fully densify the samples. Therefore our samples were not fully dense, thus likely resulting in lower mechanical properties such as in our hardness testing. Furthermore, sintering took place over 2 hours instead of the initial plan of under 30 minutes, leading to annealing and increasing grain size, also decreasing the mechanical strength of our composite. The longer sintering time may also be a result of free sintering without applied pressure.

Future Work

Several aspects of the project and areas of interest were not explored due to time and monetary constraints. A molecular dynamics model of Si sublimation and C rearrangement into

graphene were planned, but eventually rejected due to the complexity of the model. However, this simulation would give useful data on the kinetics of graphene formation rates. Additionally, future work could focus on analyzing the grain growth algorithm as it pertains to different microstructures and energy levels. Finally, several aspects of the COMSOL simulation can be improved upon. Densification considerations for SiC properties were not applied due to the lack of available and relevant data. Further analysis is also necessary to concretely determine the power-law creep parameters of SiC.

Future work can also be conducted in the experimental fabrication and densification using SPS. Due to machine limitations, the SPS at ARL was unable to apply considerable pressure during sintering. Thus, the true potential of SPS was not studied since pressure was not applied during the experimental process, leading to optimal density not being achieved in our samples.

Mechanical testing is also an important aspect in determining the viability of graphene-SiC composites for applications that require high hardness and toughness, such as ballistic armor. Due to our time constraints, only hardness values were measured. Future research would include more extensive mechanical testing in order to make definitive conclusions on the mechanical properties of SiC graphene and determine the effect of the inclusion of graphene.

Conclusions

In conclusion, the team achieved several goals and made significant process over the semester in meeting the goal of studying the fabrication of graphene-SiC ceramic composites. A model for graphene formation by the selective sublimation of Si atoms was proposed. It was determined that the necessary conditions for graphene formation are 1) vacuum or inert gas atmosphere to avoid C reaction and 2) necessary pressure and temperature that results in only the sublimation of Si atoms from SiC. A sintering model for SPS was proposed using a combination of micro/meso-scale and macro-scale simulations. Micro/meso-scale grain growth of discrete particles was modelled using a Kinetic Monte Carlo and Metropolis algorithm which simulated short range diffusion through grain boundaries, pore migration to grain surfaces, and vacancy annihilation. The results from the micro/meso-scale model were used to determine sintering parameters to be used in the macro-scale model, which utilized COMSOL. Electric currents, heat transfer, and densification were incorporated into COMSOL in order to simulate SPS processes and densification mechanisms. Appropriate boundary conditions and initial values were input based on existing literature and past research. Using the experimental voltage data from SPS runs at ARL, temperature and densification profiles were generated in COMSOL. The resulting simulation data accurately predicted the temperature during sintering. Densification results deviated from the experimental densification measurements, most likely due to both assumptions made in COMSOL as well as non-ideal experimental conditions at ARL.

For prototype fabrication, powder mixing and milling was conducted following the methods of Miranzo et al. The powders were then brought to ARL for sintering in their SPS machine following the temperature controls of Terrones. Temperature and densification were measured and compared to the simulation data.

Raman spectroscopy was used to characterize the fabricated samples. It was determined that graphene is present in all fabricated samples, confirming the results of the model and simulations. Mechanical testing included Vickers Hardness testing. However, the nature of ceramics led to widely spread out results.

Acknowledgements

References

[1] Zhang, J. and Zavaliangos, A., "Discrete Finite-Element Simulation of Thermoelectric Phenomena in Spark Plasma Sintering", Journal of electronic materials, Vol. 40, No. 5, 2011.

[2] Z. A. Munir, U. Anselmi-Tamburini, and M. Ohyanagi, "The Effect of Electric Field and Pressure on the Synthesis and Consolidation of Materials: A Review of the Spark Plasma Sintering Method," J. Mater. Sci., 41, 763–77(2006)

[3] S.H. Risbud, J.R. Groza, M.J. Kim, "Clean Grain Boundaries in AlN Ceramics Densified without Additives by a Plasma Activated Sintering Process", Phil. Mag.B, 69 (1994) 525-533.

[4] Shen, Z., Peng, H. and Nygren, M., Formidable Increase in the Superplasticity of Ceramics in the Presence of an Electric Field. Adv. Mater., 15: 1006–1009. (2003)

[5] M. Yue, J. Zhang, Y. Xiao, G. Wang, and T. Li, "New kind of Nd,Fe,B magnet prepared by spark plasma sintering", IEEE Trans. Magn., vol. 39, no. 6, pp.3551 (2003)

[6] Process for production of graphene/silicon carbide ceramic composites WO 2014047283 A1 http://www.google.com/patents/WO2014047283A1?cl=en

[7] Jae-Hwang Lee1, Phillip E. Loya1, Jun Lou, Edwin L. Thomas, "Dynamic mechanical behavior of multilayer graphene via supersonic projectile penetration", SCIENCE, Volume: 346, Issue: 6213, Pages: 1092-1096 (2014).

[8] N. Prat, F. Rongieras, J.C. Sarron; "Contemporary body armor: technical data, injuries, and limits", Eur J Trauma Emerg Surg (2012) 38:95–105. DOI: DOI 10.1007/s00068-012-0175-0.

[9] Grasso, S., Sakka, Y. and Maizza, G. "Electric Current Activated/Assisted Sintering (ECAS): A Review of Patents 1906–2008," Sci. Technol. Adv. Mater.,10, 053001 (2009).

[10] Garay, J. "Current-Activated, Pressure-Assisted Densification of Materials," An nu. Rev. Mater. Res., 40, 445–68 (2010).

[12] E. Olevsky and L. Froyen, "Constitutive Modeling of Spark-Plasma Sintering of Conductive Materials," Scripta Mater., 55, 1175–8 (2006).

[13] E. Olevsky, S. Kandukuri, and L. Froyen, "Consolidation Enhancement in Spark-Plasma Sintering: Impact of High Heating Rates," J. Appl. Phys., 102,114913 (2007).

[14] E. Olevsky, S. Kandukuri, and L. Froyen, "Analysis of Mechanisms of Spark-Plasma Sintering," Key Eng. Mater., 368–372, 1580–4 (2008).

[15] Olevsky E. and Froyen, L., "Influence of Thermal Diffusion on Spark-Plasma Sintering," J. Am. Ceram. Soc., 92, S122–32 (2009).

[16] Chaim, R. "Densification Mechanisms in Spark Plasma Sintering of Nanocrystalline Ceramics," Mater. Sci. Eng. A, 443, 25–32 (2007).

[17] Cincotti, A. "Modeling of SPS Apparatus: Temperature, Current and Strain Distribution with No Powders," AICHE J., 53, 703–19 (2007).

[18] Wang, X. "Finite Element Modeling of Electric Current-Activated Sintering: The Effect of Coupled Electrical Potential, Temperature and Stress," Acta Mater., 55, 3611–22 (2007).

[19] Antou, G, et al. "Spark Plasma Sintering of Zirconium Carbide and Oxycarbide: Finite Element Modeling of Current Density, Temperature, and Stress Distributions," J. Mater. Res., 24,404–12 (2009).

[20] Munoz, S. and Anselmi-Tamburini, U. "Temperature and Stress Fields Evolution During Spark Plasma Sintering Processes," J. Mater. Sci., 45, 6528–39 (2010).

[21] Olevsky, E:. et. al., "Fundamental Aspects of Spark Plasma Sintering: II. Finite Element Analysis of Scalability," J. Am. Ceram. Soc., 95 [8] 2414–2422 (2012).

[22] Olevsky, E. et. al., "Multi-Scale Study of Sintering: A Review," J. Am. Ceram. Soc., 89 [6] 1914–1922 (2006).

[23] Olevsky, E. "Theory of Sintering: from discrete to continuum" *Materials Science and Engineering: Reports* (1998) **23** p41-100

[24] McWilliams, B. et al. "Fully coupled thermal–electric-sintering simulation of electric field assisted sintering of net-shape compacts", J Mater Sci (2015) 50:519–530.

[25] "Engineering Design Guidelines" Saint-Gobain Ceramics. Retrieved from: http://www.hexoloy.com/high-temperature-ceramics

[26] Munro, R. "Material Properties of a Sintered alpha-SiC" Journal of Physical Chemistry. (1997). 26 p. 1195-1204.

[27] Taylor, R. and Groot H. "Thermophysical properties of Poco graphite" Air Force Office of Scientific Research (1978)

[28] "Properties and Characteristics of Graphite for industrial applications" Poco Graphite Inc. 2001.

[29] Gaskill, D.K. et al. "Epitaxial graphene growth on SiC wafers." ECS Trans. (2009). 19. P. 117-124.

[30] Lilov, S.K. "Thermodynamic analysis of phase transformations at the dissociative evaporation of silicon carbide polytypes." Diamond and Related Materials (1995). 4. p. 1331-1334.

[31] German, R. Sintering Theory and Practice, John Wiley & Sons, New York 1996.

[32] Zhou, H et al. "Creep behavior of compositionally varied SiC composites" (1997) Ceramic Engineering & Science Proceedings. 18.

[33] Anselmi-Tamburini, U. et al. "Fundamental investigations on the spark plasma sintering/synthesis process II. Modelling of current and temperature distributions" Materials Science & Engineering (2005) 394. p.139-148.

[34] Liang, H. "High electrical resistivity of spark plasmas sintered SiC ceramics with Al2O3 and Er2O3 as sintering additives" Journal of the European Ceramic Society (2015) 35. p.399-403.

[35] Guintini, D. et al. "Localized overheating phenomena and optimization of spark-plasma sintering tooling design" Materials (2013) 6. p.2612-2632

[36] Terrones, M. "Process for production of graphene/silicon carbide ceramic composites." (2014) WO2014/047283A1. U.S. Patent and Trademark Office

Appendix A: Final Budget

Item	Cost ($)
Silicon Carbide Powder (alpha, 99.8%, 2 micron) [500g]	154.00
Yitrium Oxide Powder (99.9%, <10 micron) [25g]	43.00
Aluminum Oxide Powder (99.9%, 1 micron) [25g]	17.30
Silicon Nitride Grinding Balls (x3)	123.69
USA Standard Sieve, 230 Mesh	88.40
Raman (3.75 hours)	105.00
Poster Printing	70.00
Total	**601.39**

Appendix B: Final Timeline

Name	Begin date	End date
Documentation/Reports	2/17/15	5/13/15
1st Quarterly Report / Proposal	2/17/15	2/17/15
2nd Quarterly Report	3/11/15	3/11/15
3rd Quarterly Report	4/15/15	4/15/15
4rth Quarterly Report/Final Presentat...	5/13/15	5/13/15
Sintering/Fabrication Modeling	2/18/15	5/9/15
SPS Thermal Gradient Modeling	2/18/15	3/30/15
Si Sublimation/Graphene Growth	2/18/15	3/30/15
COMSOL Verification/Debugging	3/30/15	4/27/15
Grain Growth - Kinetic Monte Carlo	4/8/15	5/9/15
Grain Growth	4/8/15	5/1/15
Pore Migration	4/23/15	5/1/15
Pore Annihilation	5/1/15	5/9/15
Analytic Ballistics Modeling	2/16/15	2/27/15
Analytic Predictions	2/16/15	3/1/15
Reliability Analysis	2/16/15	3/1/15
Order Materials	3/2/15	3/9/15
Fabrication	3/12/15	5/6/15
Powder Mixing	4/15/15	5/5/15
SPS fixed	3/12/15	3/12/15
Powder Sintering	4/15/15	5/6/15
Equipment Training	5/1/15	5/8/15
Characterization	4/27/15	5/1/15
Raman Spectroscopy	4/27/15	5/1/15
Mechanical Testing	4/29/15	5/8/15
Hardness	4/29/15	5/8/15